



# Drop on Demand Colloidal Suspension Inkjet Patterning for DIC

S. Koumlis<sup>1</sup> · S. Pagano<sup>1</sup> · G. Retuerta del Rey<sup>1</sup> · Y. Kim<sup>1</sup> · P. Jewell<sup>1</sup> · M. Noh<sup>1</sup> · L. Lamberson<sup>1</sup>

Received: 23 November 2017 / Accepted: 17 May 2018 / Published online: 9 August 2018  
© The Society for Experimental Mechanics, Inc 2018

## Abstract

Digital image correlation (DIC) is a non-contact, optical, full-field displacement measurement technique used to map deformations on a body under an applied load by tracking surface features. It is a widely used method in experimental mechanics, owed in part to its ease of setup, and applicability across length scales and material systems. Most commonly, DIC surface patterns consist of contrasting black and white speckles applied by spray paint or an airbrush, which can lack control and consistency of the distribution of speckle sizes. In this paper, drop on demand (DOD) inkjet printing of colloidal suspensions is introduced as a means to apply a speckle pattern with precision on the micro- to mesoscale. A dot array and pseudo-random DOD pattern are applied to high-density polyethylene (HDPE) specimens, tested in compression following ASTM D695-15, and compared with a traditional airbrush speckle method. The results show that the DOD pseudo-random pattern provides a more consistent strain measurement than the other two methods. The array DOD and airbrush patterns introduce erroneous signals which can be explained on the basis of two different principles. A directional pattern, such as the array DOD, is known to introduce errors in the displacement vector identification. For the random airbrush pattern, a quantification of the speckle sizes revealed a large fraction of speckles that had a characteristic length scale of around 1 pixel, which is known to introduce bias errors, since the sampling of the speckle pattern does not satisfy the Nyquist-Shannon sampling theorem. These findings illustrate the utility of DOD speckling for certain DIC applications.

**Keywords** Digital image correlation · Speckle · Drop on demand inkjet printing · HDPE

## Introduction

Digital image correlation (DIC) is a non-intrusive, optical method, mapping full-field surface displacements of a specimen [1, 2]. In its most general form, the method leverages the fact that a pattern must exist on the surface of the specimen, such as a naturally occurring texture or an artificially adhered marking. Traditionally, artificial patterns are spray painted on the surface of the specimen, resulting in a speckle pattern, such as the one shown in Fig. 1.

These patterns, natural or artificial, should contain, among other things, features of sufficient contrast that remain adhered on the surface of the specimen while it is deforming, do not stiffen the specimen, and exhibit a level of distinction from neighboring features to allow for their unique identification. The surface of the specimen of interest is then imaged using at least one digital

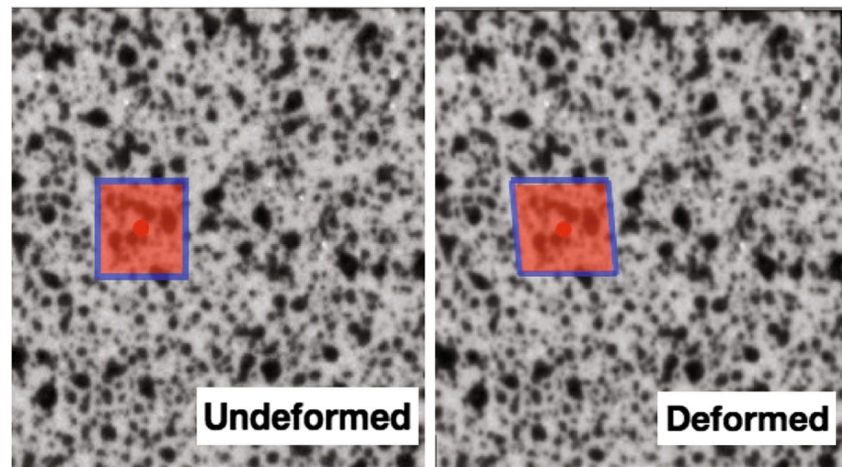
camera, in 2D DIC, or two cameras, for 3D/stereo DIC. A sequence of images is captured during the experiment, e.g. a compressive uniaxial quasi-static loading. The digital images are stored as a  $m \times n$  matrix, where  $m$  and  $n$  are the number of pixels of the camera sensor along the horizontal and vertical direction, respectively. The value of each entry of the matrix represents the grayscale level of the region of the surface imaged on the particular pixel of the sensor. The numerical value of the grayscale level depends on the bit-depth used by the camera to digitize the light intensity at each pixel, e.g. for an 8-bit digital image the grayscale values range from 0 to 255. A low grayscale level, closer to zero, represents a darker feature of the image and a higher grayscale value represents a brighter feature of the image. After the succession of images are stored digitally, a correlation criterion is used. In its most elementary form, the correlation numerical algorithm “compares” an interrogation subset of the pixels of the reference image, commonly the undeformed image, to an image that corresponds to a deformed state, as depicted in Fig. 1. This algorithm numerically estimates the location, in terms of the pixel coordinates of the center of the

✉ L. Lamberson  
les@drexel.edu

<sup>1</sup> Drexel University, Philadelphia, PA 19106, USA



**Fig. 1** Schematic of DIC deformation. The red box indicates a typical subset in both the original and deformed configuration



subset, in the deformed image. The criterion used is usually the maximum of the correlation criterion. Subsequently, the relative displacement vector between the reference and deformed configuration is computed for that particular subset, and the interrogation is repeated for another subset of the undeformed image until the whole image-matrix is interrogated and correlated. As mentioned above, contrast is an important aspect of a surface pattern leveraged to successfully employ DIC, and it represents the spread of the distribution of pixel values. One can imagine an extreme case of a featureless image, e.g. all pixels of the sensor having the same numerical value, which intuitively demonstrates that any type of correspondence/mapping from one image to the next would be unsuccessful. The output of a successful correlation computation is a full-field displacement map of the surface of the specimen. Using these displacements, the strain field can be calculated by numerical differentiation and an appropriate choice of the strain tensor [1, 3, 4]. The selected interrogation window, or subset size, should be large enough to encompass an area that includes a number of distinguishing features, making the correspondence between the reference and deformed configuration feasible [5].

One of the main reasons for the widespread use of DIC by the experimental mechanics community is the fact that it can be relatively easily executed on specimens across length scales; from the analysis of bridges or buildings [6, 7], to the deformations observed on a material loaded inside a scanning electron microscope (SEM) [8–11].

A number of different techniques have been developed to apply speckle patterns on the specimens of interest, depending on the scale of the element to be studied [12, 13]. There exists a lower bound on the size of an individual speckle, which is that the minimum size of the smallest feature in the speckle pattern should cover at least three pixels, in order to avoid ambiguities in the identification of the feature [14]. Consequently, a general rule of thumb

for DIC is that the speckles should cover at least three to five pixels on the sensor plane in order to avoid biased measurements. An intuitive way of understanding the bias error introduced in the displacement measurements is to imagine the extreme case where a feature occupies one pixel on the camera sensor in the reference configuration. Now with the slightest perturbation of the system, this same feature will be projected on two pixels on the camera sensor. This mistakenly leads the viewer, and subsequently the correlation algorithm, to assume that it is a different feature, rendering the correlation insufficient to quantify feature displacements by introducing erroneous results. This intuitive visual representation of the issues introduced by inappropriately sized speckles is only qualitative; a more accurate and quantitative determination of the error introduced can be found in Sutton et al. [3], in which it is shown that the interpolation error increases with increasing aliased content of the speckle pattern.

While it may not be immediately apparent, the absolute size of the speckle pattern, not in terms of number of pixels, but in terms of its actual physical size on the surface of the specimen, depends on the specific experimental setup. In this regard, the speckle size mainly depends on the resolution of the camera sensor, the focal length of the lens, and the field of view, or in other words the area of interest on the specimen given the overall geometry of the experimental configuration. The significance of the bias errors introduced when using inappropriately sized speckles is subtle, and must be appreciated by the experimentalist. The proper size of the speckles becomes a design problem that is specific to each application of DIC. The solution is not universal and there exists challenges in the standard methods used to create speckle patterns, e.g. spray painting. When working with larger specimen sizes, surface textures or visible features of the structure have been used as a stand-in for the speckle pattern [15, 16]. In the case of DIC under SEM and other lower length scale DIC investigations,

there has been some work embedding nano-particles on the sample surface, as well as using natural features of the sample microstructure for pattern mapping [8–11].

This paper focuses on DIC applications from the meso- to macroscale using drop-on-demand (DOD) speckling, which is a practical patterning technique for specimens between a few millimeters to a few meters in specimen size. When working on the aforementioned length scales, the most common method of patterning is manually applying the speckles. Typically, contrasting paint (binary) of black and white is applied using spray paint with resulting speckles between a few hundred micrometers and a few millimeters ( $10^{-4}$  to  $10^{-3}$  m), or by airbrush, with resulting speckles between 50 and 500  $\mu\text{m}$  depending on pressure settings and airbrush needle size, with a standard deviation on the order of 50 to 100  $\mu\text{m}$ . However, particularly at the lower length scales, certain conditions may require more precision and consistency than the size distribution of airbrushed or paint-applied speckles may provide [14]. For these cases, a novel approach to the application of speckle patterns using DOD inkjet printing with improved control and precision of the distribution of speckles is proposed, and demonstrated in this paper. The main aim of the DOD method is to take the “art” of creating speckle patterns out of the equation by providing a robust, reproducible, and easily tunable alternative to the currently existing techniques, with the aim of increasing confidence in the quantitative results obtained from DIC.

## Materials and Method

### Drop-on-Demand Inkjet Printing

The principle of operation of piezoelectric DOD is the following. A piezoelectric material interfaces with an ink-filled reservoir. By applying a specific voltage to the piezoelectric material its shape changes, creating a pressure pulse in the fluid inside the reservoir which is the driving force for an ink droplet to be ejected from the nozzle of the printer head. Software and a controller allow for precise positioning and size of the droplets. A DOD inkjet printer can generate a drop of a certain size when required. It has been used for creating microscale patterns on polymeric substrates used in micro-electromechanical systems (MEMS) fabrication [17, 18]. In this study, a DOD inkjet printer (Dimatix Material Printer DMP-2800, Fujifilm, Japan) and a piezoelectric printer head (DMC-11601, Fujifilm, Japan) were used for the generation of the pseudo-random and microdot array patterns, originating from 2D CAD drawings [19]. The patterns were printed by controlling the main printing parameters of dot size and spacing. A wide variety of colloidal solutions including conductive polymers and metallic solutions are jettable

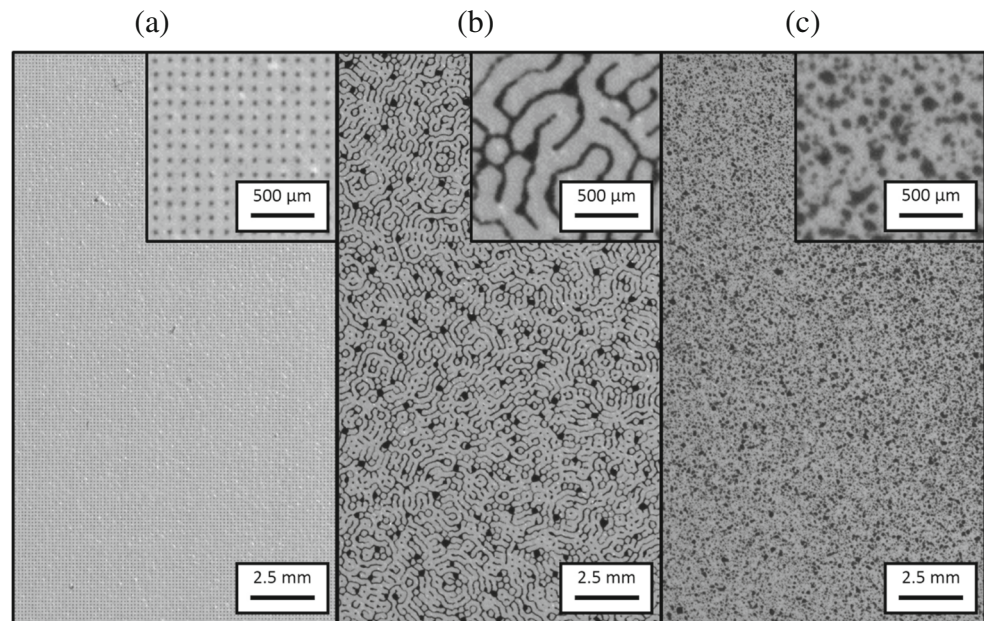
using an inkjet printer of this type. While DOD printers of this type are relatively costly, many are already employed in MEMS labs at academic institutions, and the ink used is comparatively cost-effective to traditional speckle paint for millimeter to meter-sized samples. A black ink (MFL-003, Fujifilm, Japan) was selected for this work, which is a non-toxic and non-hazardous fluid. The polymeric dye was brought into solution using a low-volatility polar solvent. The surface tension of the black ink was 28–42 mN/m and the viscosity was 11.2–11.7 centipoise at a jetting temperature of 35°C (specifications provided by the vendor). The piezoelectric printer head operates at acoustic frequencies of 1–15 kHz. A fixed frequency of 2 kHz was used for all printed patterns. The nozzle and platen temperature were fixed at 29 and 30°C, respectively. The manufacturer recommends a jetting velocity of 7–9 m/s. The jetting voltage was fixed at 21 V during printing, resulting in a drop velocity of 8 m/s. The drop spacing (DS) is the center distance between two drops and is the main parameter that determines a printed line width and uniformity. For the pseudo-random pattern, a DS of 20  $\mu\text{m}$  was used. The DOD inkjet printer and black ink was used to create the DIC patterns precisely on specimens that were painted with a uniform coating of white paint. The white base coat was cured in a conventional oven at 40°C for four hours prior to printing. It should be noted that the heating step conducted on the samples is not mandatory, and the temperature was well below the melting temperature (130°C) and away from the glass transition temperature ( $-110^\circ\text{C}$ ) of the high-density polyethylene (HDPE) [20]. This step was performed to dry the base coat faster (as the focus is not to quantify virgin material parameters, but rather to show the utility of the DOD speckle method). A comparison of the random, pseudo-random, and array patterns is provided in Fig. 2.

### Mechanical Testing and DIC Setup

Out-of-plane translation experiments were conducted for the three different speckle patterns, see Fig. 3(a). Out-of-plane translation experiments have been used to explore interpolation errors using “known” induced “strains” due to out-of-plane translation of the specimen [21]. Moving the sample away from the camera effectively produces a visual analog of a hydrostatic compression effect. Specimens with the three different speckle patterns were mounted in front of an AVT Stingray F-504b camera with a pixel resolution of  $2452 \times 2056$  and imaged with a 105 mm focal length lens. The specimen was mounted on a linear translation stage that was used to move it away/toward the camera. One image was taken every 0.25 mm of out-of-plane translation, between  $-2.5$  mm and 2.5 mm, where 0 mm corresponds to the location of the camera at optimum focus. The position of



**Fig. 2** DIC speckle patterns on the surface of HDPE specimens imaged with a 105 mm lens for further DIC analysis. **(a)** Array pattern printed using DOD inkjet printer. **(b)** Pseudo-random pattern printed with DOD inkjet printer. **(c)** Random pattern painted with airbrush technique. Insets show zoomed-in view of the full-field digital image



the linear stage was verified using a deflectometer (Epsilon 3540).

HDPE specimens, sized  $18.5 \times 18.5 \times 37$  mm, had the three different speckle patterns applied using an airbrush or DOD printing. The specimens were then deformed in uniaxial quasi-static compression with a Shimadzu AG-IC 50 kN load frame and imaged with an AVT Stingray F-504b camera with a 105 mm lens, as shown in Fig. 3(b). Prior to comparing DIC patterns, a painted HDPE specimen that was identical to those used for DIC analysis was placed in the load frame, and compressed at a rate of 1 mm/min ( $\dot{\epsilon} = 4.5 \times 10^{-4} \text{ s}^{-1}$ ) up to a maximum displacement of 4 mm ( $\approx 10\%$  strain), in order to ensure no coating failure (i.e. separation in the form of peeling or microcracking) was apparent. The resulting DIC parameters were optimized and are shown in Table 1, and all experiments were run with a target strain of 8%, or a maximum displacement of 3 mm.

Three of each of the painted and printed specimens, for a total of 9 specimens, were quasi-statically compressed, according to ASTM D695-15 [22]. The experiments were imaged during loading, and a compression plate displacement with a linear variable displacement transducer (LVDT) was used to corroborate the reference strain from the full-field imaging. MatchID software was used to correlate the obtained images and collect the full-field displacement data [23]. The analysis was performed using the software's bicubic spline interpolation function and a zero-normalized sum of squared differences (ZNSSD) correlation algorithm [23]. A performance analysis in the software was conducted to select appropriate tensor and strain window values, and the optimal strain window size of 5 subsets was used for the random and pseudo-random patterns, providing a virtual strain gage (VSG) size of 91

pixels. For the array pattern, a strain window of 13 subsets with a VSG size of 211 pixels was found to be optimal. The Euler-Almansi strain tensor was used in all cases. Note that many different options exist for analyzing DIC data such as choice of pre-filtering, interpolation schemes, etc. Some optimal choices have been suggested in literature that minimize systematic errors [24] and produce robust results with minimized sensitivity on experimental factors. In this work, in order to exemplify the effect of the speckle pattern on systematic errors, some of these parameters have been adjusted and results are compared for different choices of interpolation functions and pre-filtering options. Unless otherwise specified, the DIC parameters presented in Table 1 are the default choices.

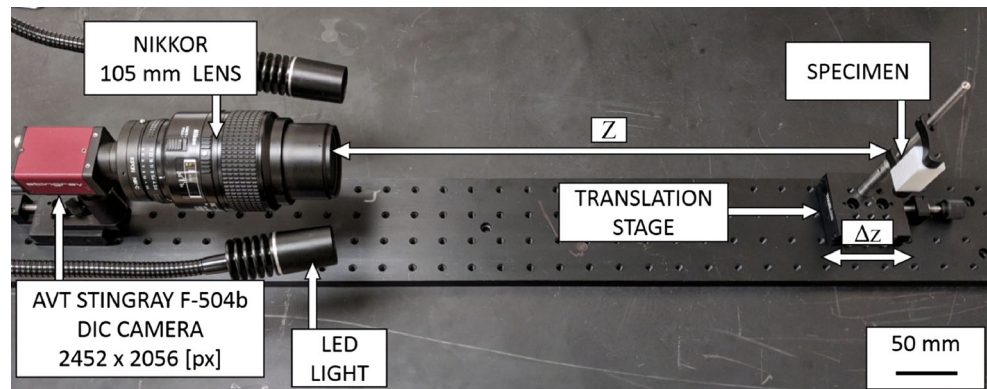
## Results and Discussion

### Speckle Size and Pattern Contrast Analysis

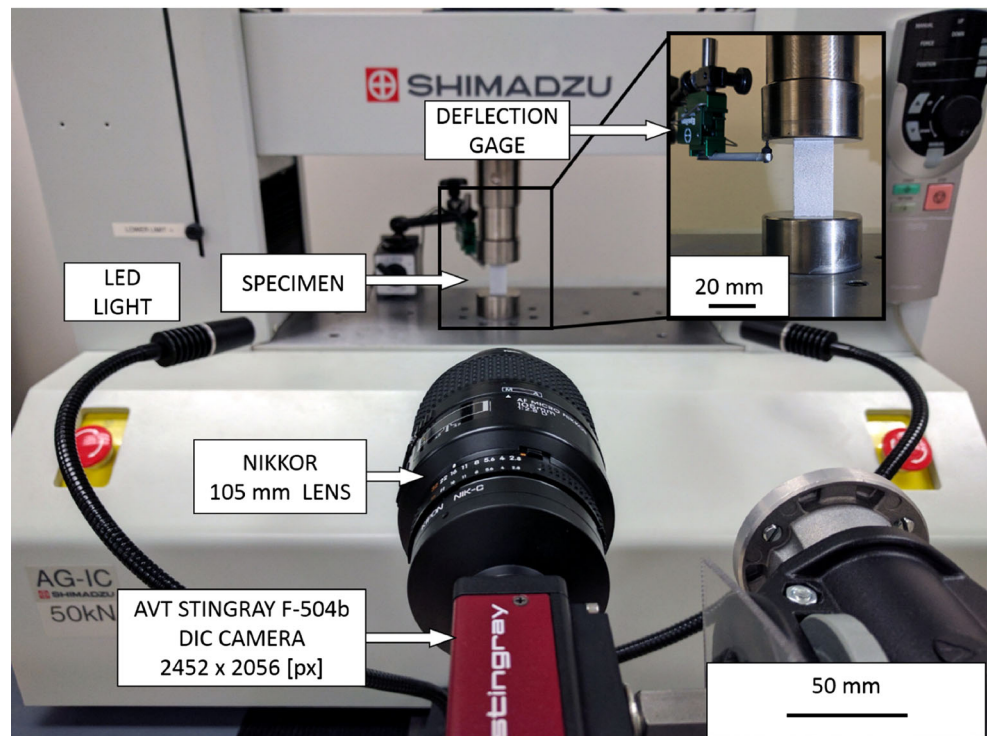
In order to quantify the distribution of feature sizes, each of the three speckle types were analyzed using a MATLAB code modified from a similar approach developed to measure the fragment size and distributions of dynamically loaded brittle materials; details found in Pagano et al., among others [25–27].

In the case of the random pattern and array pattern, the feature size was measured as the diameter of an individual dot in the speckle. The pseudo-random pattern could not be analyzed using this approach as there is no standard circular stand-alone shape. Instead, the feature size considered is the minor axis length of an ellipse fit to each feature shape. The result of this analysis is provided as a histogram in

**Fig. 3** (a) Out-of-plane translation experimental setup showing camera, lens, lighting, translation stage, and specimen. (b) Experimental setup used during the test showing imaging system and LED lighting. Inset: HDPE specimen, sized  $18.5 \times 18.5 \times 37$  mm, in testing configuration



(a)



(b)

Fig. 4, where each distribution was normalized by dividing the individual frequencies by the total number of features obtained for that pattern, and thus the vertical axis of the histogram represents the relative frequency. The histograms indicate that the array pattern had the most consistent printing of features with the “narrowest” distribution out of the three different patterns, whereas the randomly applied paint pattern produced the largest spread of feature sizes with bimodal distribution characteristics [28]. Moreover, it can be observed that almost 30% of the random pattern features, i.e. the pattern produced by using the airbrush, had sizes between 15 and 25  $\mu\text{m}$ . As given by the information provided in Table 1, the pixel size of the experimental setup falls within this range, which implies that a bias error in

the displacement measurements when using this speckle pattern technique for DIC will be introduced (see discussion in “Introduction”). Also note that the average characteristic length for the pseudo-random pattern can be easily dialed-in with the DOD method, and it is consistent with the targeted size when designing the experiment.

An important property of a speckle pattern is the average contrast in each subset, which is a measure of the information content in each subset. Five static images were taken for each pattern and averaged to reduce any artifacts on the obtained contrast values due to inherent noise of the camera sensor [29]. The averaged images of the three patterns were then processed to calculate the average contrast value for each subset of the pattern using the sum

**Table 1** DIC parameters used for the analysis of the data obtained from the compression tests on HDPE specimens

| DIC Parameters    |                       |       |
|-------------------|-----------------------|-------|
| Camera model      | Stingray F-504B       | –     |
| Lens              | NIKKOR 105 mm f/2.8 D | –     |
| Sensor array size | 2452 × 2056           | px    |
| Interframe time   | 500                   | ms    |
| Pixel size        | 18                    | μm/px |
| Feature size      | 55                    | μm    |
| Spacing           | 110                   | μm    |
| Software          | MatchID v2017.2.0     | –     |
| Algorithm         | ZNSSD [23]            | –     |
| Interpolation     | Bicubic spline        | –     |
| Shape function    | Affine                | –     |
| Prefiltering      | None                  | –     |
| Subset size       | 31                    | px    |
| Step size         | 15                    | px    |

square of the gradients,  $\sqrt{\sum_{i=1}^N \sum_{j=1}^N [\nabla I(x_{ij})]^2}$ , where  $N$  is the subset size, and  $I(x_{ij})$  is the gray-level intensity value of pixel  $(i, j)$ . The average contrast for each subset of the three different patterns is shown as a map at the bottom of Fig. 4. It can be seen that the pseudo-random DOD pattern encodes features of higher contrast within each subset when compared against the average subset contrast levels of the random and array DOD patterns. It is known that for a

given noise level, higher contrast leads to lower DIC errors [29, 30] and it is anticipated that this will have an effect on the accuracy of the DIC values obtained using the three different patterns.

### Out-of-Plane Translation

To quantify the bias interpolation error due to aliased speckle content, out-of-plane translation experiments were conducted [21, 31]. The strain maps for the three different patterns, along with line-plots of strain versus location, are shown in Figs. 5 and 6, for a bi-linear polynomial and a bi-cubic spline interpolant, respectively. The results shown are for an out-of-plane translation of  $\Delta z = 1.25$  mm away from the camera, which effectively simulates an in-plane hydrostatic compression of around 5 pixels. The strain field is expected to be uniform, with a strain magnitude equal to  $\varepsilon_{nn} = \frac{\Delta z}{Z}$ , where  $n$  denotes either one of the two in-plane strain components, and  $Z$  is the distance between the object and the camera [31]. The two dashed lines represent the bounds of the theoretically expected strain value. The upper bound represents the strain amplitude in the case where  $Z$  is taken to be the distance from the sample to the camera body, whereas the lower bound is obtained by measuring the distance  $Z$  from the sample to the front of the lens. As seen in Figs. 5 and 6, banding in the strain maps is observed for all three speckle pattern cases. These strain oscillations are systematic errors that have been attributed to aliased content of the speckle pattern. A reduction of

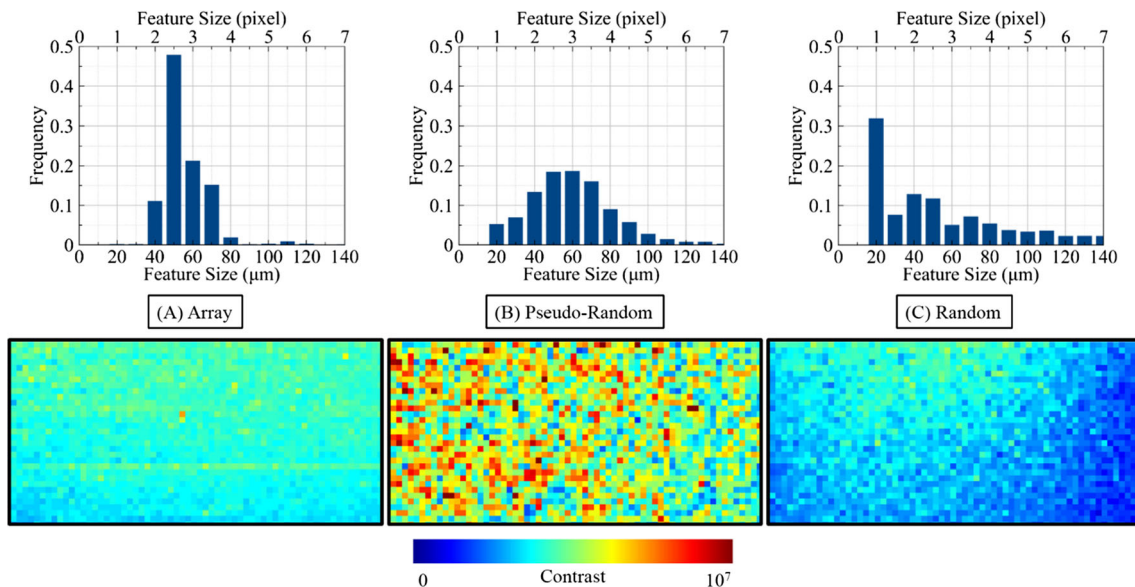


**Fig. 4** Top row: Histograms of different speckle patterns showing the speckle size distribution for the array, pseudo-random and random patterns printed on HDPE specimens. Bottom row: Maps of average subset contrast for the three different speckle patterns

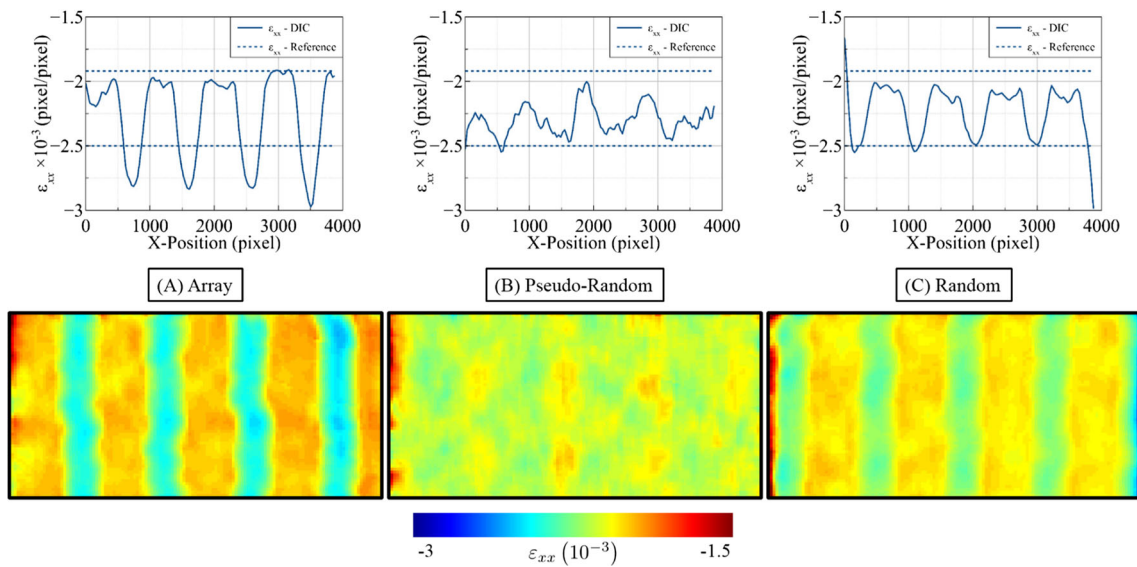


**Fig. 5** Out-of-plane translation of  $\Delta z = 1.25$  mm. (Top row) Strain line-plots and (bottom row) strain maps for the three different speckle patterns using a **bi-linear polynomial interpolant**. Dashed lines represents the bounds of the theoretically expected strain field amplitude

the strain oscillation amplitude is observed when using a bi-cubic spline interpolant function, Fig. 6, compared to a bi-linear polynomial interpolation function, Fig. 5, for all three patterns. The array pattern exhibits the highest strain oscillations, whereas the pseudo-random DOD pattern is the most robust of the three patterns showing the least amount of banding for any choice of interpolant.

### Comparison of Speckle Patterns: Average Strain

With 2D DIC, full-field in-plane displacements on the specimen’s surface are mapped, and strain fields correspondingly measured. However traditionally with a compression load-frame, an averaged or point measurement of displacement across the whole specimen is taken by an LVDT

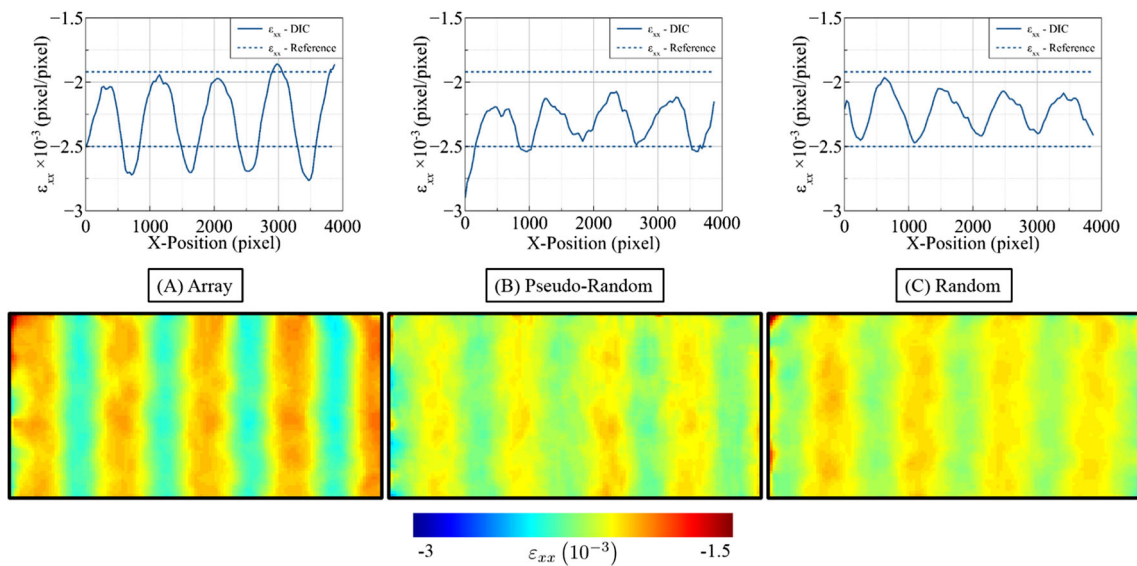


**Fig. 6** Out-of-plane translation of  $\Delta z = 1.25$  mm. (Top row) Strain line-plots and (bottom row) strain maps for the three different speckle patterns using a **bi-cubic spline interpolant**. Dashed lines represents the bounds of the theoretically expected strain field amplitude

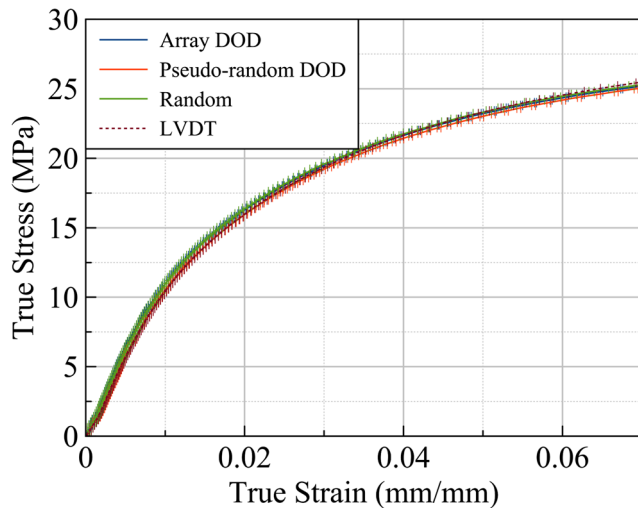


**Fig. 7** Combined plot showing average stress-strain response of HDPE at  $\dot{\epsilon} = 4.5 \times 10^{-4} \text{ s}^{-1}$  using random, pseudo-random DOD, and array DOD, speckle patterns for DIC results and an LVDT sensor for reference

or extensometer gage. This method of measurement, like a strain gage, is a point-wise type measurement, whereas DIC allows for a wealth of information given the ability to map the entire specimen surface of interest. That said, for the sake of comparison, an average strain over the field of view is taken from the DIC speckle techniques under uni-axial quasi-static compression of HDPE specimens, and compared with the “reference” value provided by the LVDT.

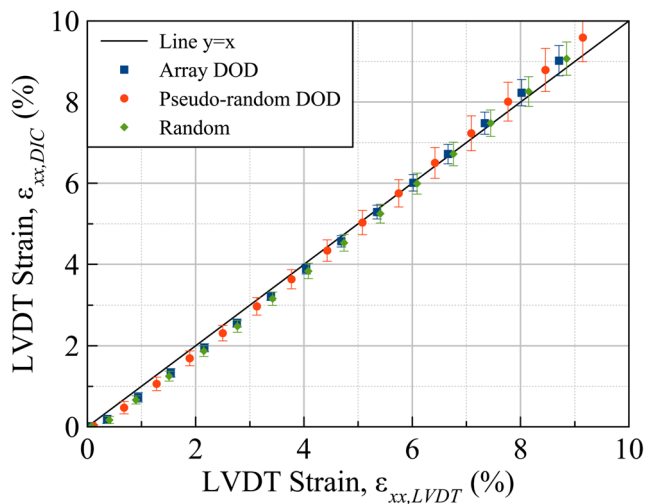


**Fig. 8** Comparison between DIC and LVDT measurements of strain in the loading, or x-direction. The line  $y = x$  indicates agreement between the two measurements. The error-bars represent standard deviation values for the strain across the entire field of view

Figure 7 shows the mean true stress and true strain curves for the three different patterns. The results of the average stress-strain response obtained by using the three different speckle patterns and DIC compare well with the “reference” values obtained from the LVDT measurements. There is no significant difference between the DIC and LVDT results. The average stress-strain response from this comparison appears to be insensitive to the speckle pattern used.

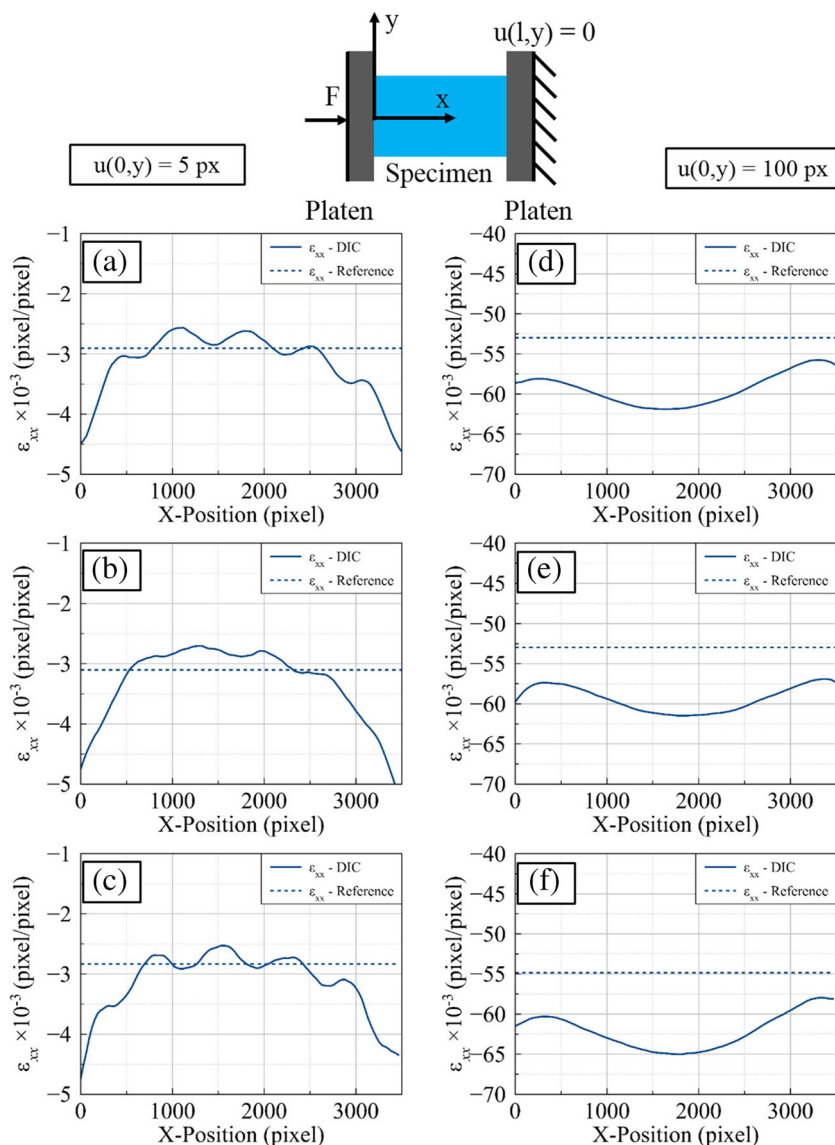
As the DIC and the LVDT methods were used concurrently during the experiments, the strain measured from the two different methods can be compared side by side. This is shown in Fig. 8, where the average strain along the loading direction, labeled here as the x-direction, is plotted for the three different speckle patterns versus the corresponding measurement from the LVDT gage. Error-bars represent the standard deviation of the strain values across the whole field of view. Deviation of the scatter plot points from the  $y = x$  line indicates disagreement between the two measurements. As can be seen in Fig. 8 the average strain values obtained with the different methods nominally agree with each other.

### Comparison of Speckle Patterns: Full-Field

As demonstrated in the previous section, the quantification of the stress-strain response of the specimen was insensitive to the choice of speckle pattern used, in the average sense. In this section, a comparison of the full-field strain measurements obtained from the different speckle patterns is presented, as shown in Fig. 9. At the top of Fig. 9, a schematic of the experimental setup is shown, with the loading direction (x-direction) flipped horizontally for ease of viewing. For a homogeneous material under uniaxial compression, one would expect a homogeneous strain response sufficiently far away from the loading surfaces. In the ideal sense, the results would be measuring a homogeneous, i.e. constant, strain map at each instant of loading across the full-field of view on the specimen,  $\epsilon_{xx} = C$ . In the left column of Fig. 9, line-plots of the horizontal strain component,  $\epsilon_{xx}$ , as a function of the x-location along the specimen are shown for the three different patterns, at a compression of 5 pixels. For the array and random patterns, Fig. 9(a) and (c), a bias strain is observed, similar to the one observed during the out-of-plane displacement experiments. The bias error is the smallest for the pseudo-random DOD pattern, Fig. 9(b), and maximum for the array pattern, Fig. 9(a). A bi-cubic spline interpolant has been used, since in the out-of-plane displacement experiments it was demonstrated that this interpolant is the better-behaved one. Results using the bi-linear polynomial interpolant exhibited



**Fig. 9** Line-plots of strain versus x-location for a quasi-static 5 pixel compressive deformation of HDPE specimens using the (a) array (b) pseudo-random (c) and random speckle pattern. Line-plots of strain versus 100 pixel location for a quasi-static 100 pixel compressive deformation of HDPE specimens with an (d) array (e) pseudo-random (f) and random speckle pattern. The dashed lines represent the reference strain value



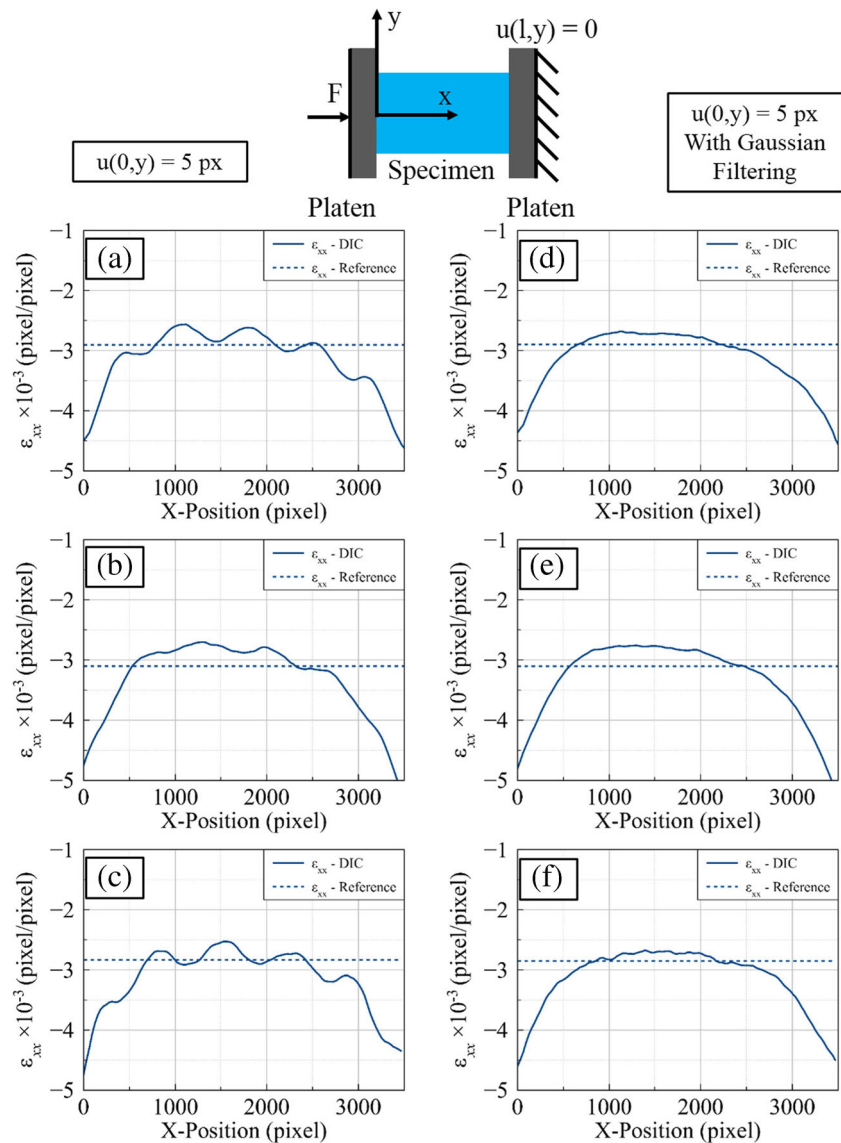
higher amplitude oscillations around the average strain level compared to the bi-cubic spline and are not shown here. In the right column of Fig. 9 similar line-plots are shown but for a much larger compressive displacement of 100 pixels. The strains at this higher compressive state are identical for the three different patterns. The bias error is significant for small deformations, but not for larger ones.

The effect of pre-filtering on the bias error was also investigated. In the results shown thus far, no pre-filtering of the speckle pattern was applied. The same experimental data obtained from quasi-static compressive experiments was processed by the same algorithm, but this time a Gaussian pre-filtering step with a Kernel size of 5 pixels was

incorporated. The left column of Fig. 10 shows the results at a 5 pixel compression without pre-filtering, whereas the results on the right column show the same experimental data, but analyzed after applying a Gaussian filter. Pre-filtering the gray-level intensity values of the raw images seems to minimize the systematic interpolant errors for all three different patterns. Nevertheless, the pseudo-random DOD pattern seems to be the most robust pattern that is insensitive to the choice of DIC parameters, such as interpolation function used and pre-filtering options. This fact demonstrates the ability of the DOD technique to apply speckle patterns of high-quality that can be used with confidence for DIC metrology.



**Fig. 10** Line-plots of strain versus x-location for a quasi-static 5 pixel compressive deformation of HDPE specimens using the (a) array (b) pseudo-random (c) and random speckle pattern using no pre-filtering. The same line-plots of strain versus location for a quasi-static 5 pixel compressive deformation of HDPE specimens with an (d) array (e) pseudo-random (f) and random speckle pattern using a Gaussian pre-filter with a kernel size of 5 pixels. The dashed lines represent the reference strain value



## Conclusion

By implementing the DOD inkjet printing technique, the DIC pattern features sizes and spacings are easily tunable, and the resulting pattern is highly reproducible. Given this control, any bias error introduced in the DIC analysis from improperly sized speckles can be avoided, leading to patterns that can be used with higher confidence to obtain quantitative DIC measurements. In particular for the presented case, the random speckle pattern, produced by painting the surface with an airbrush, resulted in 30% of the speckles (dots) sizes on the order of 1 pixel. The size distribution of the speckles is more difficult to control when using spray paint or airbrush techniques, resulting in the potential to obtain undersized speckles which can lead to aliasing by violation of the Nyquist-Shannon sampling theorem. Such aliasing errors are, in general, quite difficult

to detect. Moreover, the pseudo-random DOD pattern exhibits the highest average contrast per subset which is known to reduce errors in DIC [29, 30].

Out-of-plane translation experiments are suited for quantifying the interpolant errors in DIC, as demonstrated in the work of Reu et al. [21]. A series of out-of-plane translation experiments helped elucidate the superior quality of the pseudo-random DOD speckle pattern when compared to the array DOD and random airbrushed speckle patterns. It was shown that for the interpolant used, spline or polynomial, the pseudo-random DOD pattern exhibited the lowest interpolant error.

The average stress-strain response of the HDPE specimens subjected to quasi-static uniaxial compression experiments was found to be insensitive to the speckle pattern used, and all DIC results matched those obtained with the reference LVDT point measurement. In order to further

investigate the influence of the DIC pattern on the full-field data, line-plots were extracted from the full-field strain maps. For a small compression of about 5 pixels, a strain error that appeared as banding, or in other words an oscillating strain field, was observed. The banding was worse for the array and random speckle patterns and appeared to be minimal for the pseudo-random DOD pattern. At higher strains, around 100 pixel crush, the banding disappeared and there was no significant difference between the three different speckle patterns. The effect of pre-filtering on the obtained strain fields was shown to be significant.

The 5 pixel Kernel Gaussian pre-filtering reduced the interpolation errors, which can be attributed in smoothing-out, or softening, the speckles' edges [32]. Even for the array pattern that does not have aliased content, the hard edges of the speckles have a frequency content that is impossible to fully-resolve. Consequently, using “well behaved” DIC parameters, such as interpolation functions and pre-filtering options, can minimize the bias errors that may be introduced from speckle pattern with questionable quality. Nevertheless, this work demonstrated that the DOD speckle technique is a well founded method to control the pattern features, capable of creating a robust pattern that shows minimal sensitivity to the DIC analysis parameters chosen.

Moreover, since DIC analysis provides full-field surface deformation and strain maps, there are essentially no limitations to using the DOD method on different material systems, e.g. isotropic, orthotropic, heterogeneous, etc, if the surface can be painted. The DOD method allows for the speckle pattern to be precisely controlled, which in turn establishes confidence on the measured full-fields that directly relate to behavior of the underlying material (with the same confidence as more traditional spray paint speckle methods), and are not systematic error artifacts (e.g. banding of strain measurements) due to poor quality speckles.

**Acknowledgments** The authors would like to gratefully acknowledge support of this research through the American Chemical Society Petroleum Research Fund No. PRFSS860-ND10, the Office of Naval Research Young Investigator Award No. N00014-17-1-2497, the National Science Foundation Award No. 1636190, and the Office of Naval Research Award No. N00014-17-2644.

## References

- Sutton M, Wolters W, Peters W, Ranson W, McNeill S (1983) Determination of displacements using an improved digital correlation method. *Image Vis Comput* 1(3):133–139
- Schreier H, Orteu J-J, Sutton MA (2009) *Image correlation for shape, motion and deformation measurements*. Springer, New York
- Sutton MA, Orteu JJ, Schreier H (2009) *Image correlation for shape, motion and deformation measurements: basic concepts, theory and applications*. Springer Science & Business Media, Berlin
- Reu P (2015) DIC: a revolution in experimental mechanics. *Exp Tech* 39(6):1–2
- Daly SH (2010) Digital image correlation in experimental mechanics for aerospace materials and structures. In: *Encyclopedia of aerospace engineering*. American Cancer Society. <https://doi.org/10.1002/9780470686652.eae542>
- Yoneyama S, Kitagawa A, Iwata S, Tani K, Kikuta H (2007) Bridge deflection measurement using Digital Image Correlation. *Exp Tech* 31(1):34–40
- Hoult NA, Take WA, Lee C, Dutton M (2013) Experimental accuracy of two dimensional strain measurements using Digital Image Correlation. *Eng Struct* 46:718–726
- Kammers A, Daly S (2011) Small-scale patterning methods for Digital Image Correlation under scanning electron microscopy. *Meas Sci Technol* 22(12):125501
- Sutton MA, Li N, Garcia D, Cornille N, Orteu JJ, McNeill SR, Schreier HW, Li X (2006) Metrology in a scanning electron microscope: theoretical developments and experimental validation. *Meas Sci Technol* 17(10):2613
- Sutton MA, Li N, Joy D, Reynolds AP, Li X (2007) Scanning electron microscopy for quantitative small and large deformation measurements part i: SEM imaging at magnifications from 200 to 10,000. *Exp Mech* 47(6):775–787
- Sutton MA, Li N, Garcia D, Cornille N, Orteu J, McNeill S, Schreier H, Li X, Reynolds AP (2007) Scanning electron microscopy for quantitative small and large deformation measurements part II: experimental validation for magnifications from 200 to 10,000. *Exp Mech* 47(6):789–804
- Lane C, Burguete RL, Shterenlikht A (2008) An objective criterion for the selection of an optimum dic pattern and subset size. In: *Proceedings of the XI<sup>th</sup> International Congress and Exposition*, pp 1–9
- Bossuyt S (2013) Optimized patterns for Digital Image Correlation. In: *Imaging methods for novel materials and challenging applications*. Springer, vol 3, pp 239–248
- Reu P (2014) All about speckles: speckle size measurement. *Exp Tech* 38(6):1–2
- Malesa M, Szczepanek D, Kujawińska M, Świercz A, Kołakowski P (2010) Monitoring of civil engineering structures using Digital Image Correlation technique. In: *EPJ web of conferences*. EDP Sciences, vol 6, p 31014
- Gamache R, Santini-Bell E (2009) Non-intrusive digital optical means to develop bridge performance information. In: *Non-destructive testing in civil engineering*, pp 1–6
- Kim Y, Ren X, Kim J, Noh H (2014) Direct inkjet printing of micro-scale silver electrodes on polydimethylsiloxane (PDMS) microchip. *J Micromech Microeng* 24(11):115010
- Kim Y, Kim JW, Kim J, Noh M (2017) A novel fabrication method of parylene-based microelectrodes utilizing inkjet printing. *Sensors Actuators B Chem* 238:862–870
- Fujifilm Dimatix (2016) *Dimatix Materials Printer DMP-2850 Datasheet, Rev. 03 Edition*
- Martienssen W, Warlimont H (2006) *Springer handbook of condensed matter and materials data*. Springer Science & Business Media, Berlin
- Reu PL, Toussaint E, Jones E, Bruck HA, Iadicola M, Balcaen R, Turner DZ, Siebert T, Lava PL, Simonsen M (2017) DIC challenge: developing images and guidelines for evaluating accuracy and resolution of 2D analyses. *Exp Mech* 3:1–33
- ASTM D695-15 (2015) *Standard test method for compressive properties of rigid plastics*, ASTM International, Standard, ASTM International, West Conshohocken, PA



23. Lava P, Debruyne D (2010) MatchID
24. Schreier HW, Hubert W, Joachim R, Sutton MA (2000) Systematic errors in digital image correlation caused by intensity interpolation. *Opt Eng* 39(11):2915–2922
25. MATLAB (2016), version, 9.1.0 (R2016b), The MathWorks Inc., Natick, Massachusetts
26. Pagano S, Hogan J, Lamberson L (2016) Bone and bone surrogate fragmentation under dynamic compression. *Journal of Dynamic Behavior of Materials* 2(2):234–245
27. Hogan JD, Rogers RJ, Spray JG, Boonsue S (2012) Dynamic fragmentation of granite for impact energies of 6–28J. *Eng Fract Mech* 79:103–125
28. Lecompte D, Smits A, Bossuyt S, Sol H, Vantomme J, Van Hemelrijck D, Habraken A (2006) Quality assessment of speckle patterns for Digital Image Correlation. *Opt Lasers Eng* 44(11):1132–1145
29. Reu P (2015) All about speckles: contrast. *Exp Tech* 39(1):1–2
30. Pan B, Lu Z, Xie H (2010) Mean intensity gradient: an effective global parameter for quality assessment of the speckle patterns used in digital image correlation. *Opt Lasers Eng* 48(4):469–477
31. Sutton MA, Yan JH, Tiwari V, Schreier HW, Orteu J (2008) The effect of out-of-plane motion on 2D and 3D digital image correlation measurements. *Opt Lasers Eng* 46(10):746–757
32. Reu P (2015) All about speckles: edge sharpness. *Exp Tech* 39(2):1–2

